

# A model of the electric field in a one-dimensional micro-mirror array and electromechanical simulations and optimization in a single cell

Duy Duc Nguyen<sup>1</sup>, Nguyen Nhat Binh Trinh<sup>1</sup>, Michel Lenczner<sup>1</sup>, Frédéric Zamkotsian<sup>2</sup>, and Scott Cogan<sup>1</sup>

<sup>1</sup>FEMTO-ST, University of Bourgogne Franche-Comté, CNRS, UTBM, Besançon, France.

<sup>2</sup>LAM-CNRS, Marseille, France.

Email : [duyduc.nguyen@femto-st.fr](mailto:duyduc.nguyen@femto-st.fr), [nhat-binh.trinh@femto-st.fr](mailto:nhat-binh.trinh@femto-st.fr), [michel.lenczner@femto-st.fr](mailto:michel.lenczner@femto-st.fr), [frederic.zamkotsian@lam.fr](mailto:frederic.zamkotsian@lam.fr), [scott.cogan@univ-fcomte.fr](mailto:scott.cogan@univ-fcomte.fr)

## Abstract

This paper reports recent progress in modeling and simulation of a one-dimensional Micro-Mirror Array actuated by an electrostatic force. We present results obtained through numerical simulations of a single cell: the analysis and the optimization of the pull-in voltage and the analysis of the bounces of the mirror in contact with the base when it is subjected to a voltage exceeding the pull-in voltage. For the array, a model has been derived for the electrostatic field using a multi-scale modeling technique. The model is detailed together with simulation results.

**Keywords.** *Micro-Mirror Array, Periodic Homogenization, Pull-In Voltage Analysis, Bouncing Effect, Robust Optimization*

## 1. Introduction

The Micro-Mirror Array (MMA), MIRA, considered in this paper and shown in Figure 1 is dedicated to applications in astrophysics, and has been developed in a collaboration between the LAM and the CSEM (Switzerland), see [1, 2] and Figure 1. It is designed to play the role of a field selector for multi-object spectroscopy (MOS) in that it allows for individual selection of objects by preventing overlapping of spectra, and that it removes spoiling sources and background emission. The actuation principle is based on the attraction of the suspended mirror towards the bottom electrode by an electrostatic force generated by their difference of potential. The spring force of the suspending beams is a restoring force to get back the mirror in its rest position.

In the first third of the gap between the mirror and the electrode, the position of the mirror can be controlled by the voltage. But for the lower position, the system becomes unstable and the mirror is completely attracted towards the electrode. The related voltage is called *pull-in voltage*. The pull-in analysis is carried out by using COMSOL Multi-Physics, and latter compared with numerical results in [2] done by using CoventorWare.

Once simulation is available, many optimization can be envisioned, some of them that are interesting from the designer point of view such as: to minimize the restoring force of the beams, to minimize the pull-in voltage, to reach the correct tilt angle of the mirror or to minimize the speed of the mirror leaving the landing pad during the pull-out process. Here, we report results on the minimization of the pull-in voltage depending on the two most influential parameters, namely the suspending beam thickness and length. This work is done by using an in-house optimization software package SIMBAD. Due to the model simulation

time, the optimization is conducted on a meta-model based on a sample of 25 simulations.

Then, the dynamical mirror stabilization process has been studied through the *bouncing effect* in vacuum that is the bounces of the landing beams that touch the landing pads.

The full modeling of the MMA should cover mechanical, electrical and thermal effects. However, a direct simulation of any of them in such MMA turns out to be impractical, since the MMA has a complex geometry and a large number of cells. In [3], we have already introduced a multi-scale model for heat transfer occurring in an one-dimensional array of micro-mirrors. In this paper, we focus on the electrostatic field in the array. Due to the presence of imposed voltages in each cell, the structure of the model differs from usual homogenized models in that there is no global variation of the electrical field. Precisely, the solution of this model is a sum of a periodic electric potential and boundary layer potentials occurring at the two ends as well as at the possible interfaces between regions of different applied voltages. The multi-scale modeling method is based on the framework of periodic homogenization as in [4].

The resulting model is implemented in COMSOL thanks to the Partial Differential Equations (PDEs) interface. All parts of the model are computed using a very number of cells. Their solutions are combined in a single plot to represent the full solution of the electrostatic field in the MMA. Therefore, computing the solution for a large array has no limitation with this model. The assembly of the solutions of the model parts is achieved thanks to the LiveLink package linking MATLAB and COMSOL.

## 2. Description of the Micro-Mirror Array

The structure of this MMA is detailed in [2]. Figure 2 shows the parts of its elementary cell which is divided into two elements: the mirror with voltage  $+V$  and the electrode with voltage  $-V$ . The mirror part is composed of the mirror, two stopper beams with two landing beams on their tips and a suspending beam. The electrode part is composed of an electrode, two landing pads and two pillars.

Each cell can be addressable by applying different voltages on its line and column and then tilted due to the generation of electrostatic force on the mirror, [1, 2]. At rest, when no voltage is applied, the micro-mirror is held in a flat position by the suspended beams. When a voltage difference  $2V$  is applied between the micro-mirror and the electrode, an electrostatic force is generated, resulting in the at-

traction of the micro-mirror toward the fixed electrode, and leading to tilting. For voltages below the pull-in voltage, the micro-mirror is operated in an analogue mode, allowing the angle to be set to a few degrees as a function of the applied voltage. At the pull-in voltage, the force increases and the micro-mirror snaps toward the electrode. During this motion, the micro-mirror touches its stopper beam and its landing pads. After pull-in, the micro-mirror is fixed at a precise tilt angle, due to contact with three points, the stopper beam and two landing pads. When the voltage is reduced, the micro-mirror angle remains constant until the mirror detaches from its stopper beam and increased its tilt angle. Finally, when the spring force of the suspended beams overcomes the electrostatic force, the landing beams detach from the landing pads and the mirror returns to its rest position.

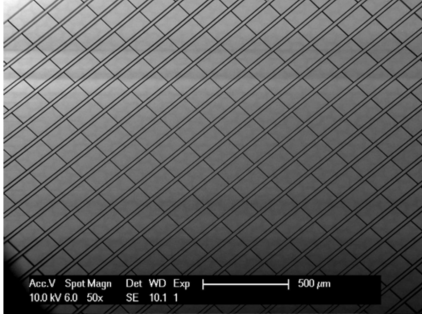


Fig. 1: Top view of MIRA a micro mirror array made with  $64 \times 32$  cells of size  $100 \times 200 \mu\text{m}^2$ .

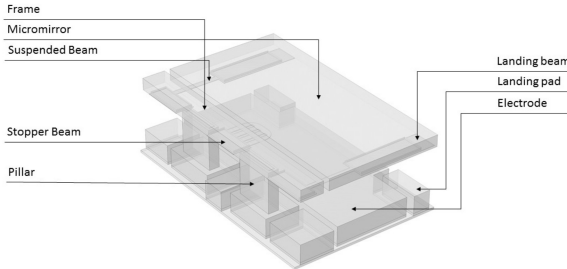


Fig. 2: The parts of a cell of MIRA.

### 3. Pull-in analysis

The computation of the pull-in voltage  $V_{pi}$  is done by solving an inverse problem. The pull-in voltage is found by imposing the mirror end at successive predefined positions starting from the rest position and ending to a displacement equal to the third of the gap. For each position, the voltage is adjusted to cancel the applied force by imposing the displacement. The choice of an initial displacement close to zero and of a sufficiently small displacement step are to guarantee correct convergence of the nonlinear solver, provided that each new computation starts with an initial condition built from the previous result. The higher position requires the largest voltage, but in turn, the lower position increases the electrostatic force and thereby requires a lower voltage. As a result, the plot of the voltages versus the positions is a parabola in which the maximum corresponds to the pull-in voltage. Figure 3 shows the voltage-displacement

curves of the micro-mirror at equilibrium. Table 1 shows the variation of  $V_{pi}$  for different values of the thickness  $t$  and the length  $\ell$  of the suspended beam. These results are in agreement to those of [1, 2]. We observe that the key parameter is the beam thickness and that the beam thickness must be lower than  $500\text{nm}$  for a pull-in voltage below  $100\text{V}$ .

$t$ and $\ell$	$40 \mu\text{m}$	$60 \mu\text{m}$	$80 \mu\text{m}$
$400 \text{ nm}$	$87 \text{ V}$	$81 \text{ V}$	$82 \text{ V}$
$500 \text{ nm}$	$120 \text{ V}$	$115 \text{ V}$	$115 \text{ V}$
$600 \text{ nm}$	$157 \text{ V}$	$150 \text{ V}$	$154 \text{ V}$

Table 1: The pull-in voltage as a function of the length and thickness of the suspended beams.

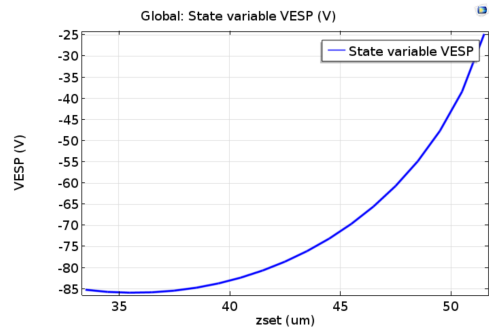


Fig. 3: Curve of imposed voltage versus beam displacement at equilibrium for supporting beams with thickness  $400\text{nm}$  and length  $40\mu\text{m}$ .

### 4. Optimization of the pull-in voltage

The optimization of the pull-in voltage  $V_{pi}$  is a single objective optimization problem with two design variables  $t$  and  $\ell$ . The optimization procedure is speed up thanks to a meta model. The latter is built by sampling the two variables  $t$  and  $\ell$  with 25 samples corresponding to 5 values of  $t = \{0.4, 0.45, 0.5, 0.55, 0.6\} \mu\text{m}$  and 5 values of  $\ell = \{40, 50, 60, 70, 80\} \mu\text{m}$ . The meta-model is chosen as a fourth order polynomial interpolation. The graph of the meta-model is shown in Figure 4. The mean square error is 1.8%. We observe that the main slope is in the direction of  $t$  while the surface is flat in the direction of  $\ell$  meaning that the most sensitive variable is the beam thickness.

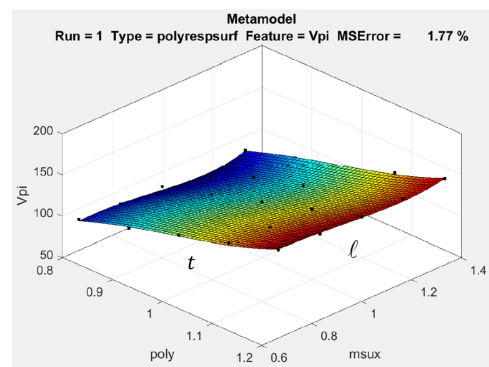


Fig. 4: The meta-model of the pull-in voltage as a function of the length ( $\ell$ ) and thickness ( $t$ ) of the suspended beams.

The minimization of the pull-in voltage performed with the meta-model is reached for  $t = 400 \text{ nm}$  and  $\ell = 70.16 \mu\text{m}$ , see Table 2.

Design Variable	Initial Value	Optimal value
$t$	500 nm	400 nm
$\ell$	60 $\mu\text{m}$	70.16 $\mu\text{m}$
Feature		
$V_{PI}$	115.2 V	74.4 V

Table 2: The initial and optimal values of the design variables  $t$ ,  $\ell$  and of the optimization objective  $V_{PI}$ .

## 5. Bumping effect

The simulations of the mirror bounces are done using the electromechanical interface of COMSOL in the dynamic regime for a two-dimensional geometry. The contact between the landing beams and the landing pads together with the contact between the mirror and the stopper beam are handled by an approximate penalty or barrier method, as described in [5]. Precisely, nonlinear spring forces  $F_c$  are used for modeling the elastic contact between the landing pads and a part of the mirror surface and the stopper beam, see Figure 5. When these surfaces are moved away from each other, the springs have a low stiffness and consequently a negligible influence on the deformation of the beam and the mirror. As the gap is reduced the springs become stiffer and resist to the gap closure, see Figure 6.

The results of Figure 7 show that there is almost no bounce when the beam thickness is lower than  $1\mu\text{m}$ , while the results of Figure 8 show a few bounces when the beam thickness is greater than  $1\mu\text{m}$ . This difference of behavior is due to a weaker spring force, indeed the restoring force of a thin ( $0.7\mu\text{m}$ ) beam is weak, leading to a fast tilt actuation and fast stabilization. In the opposite, when the beam thickness is larger ( $1\mu\text{m}$ ), the time scale of the restoring force is longer, and the tilting time is also longer with many bounces before stabilization.

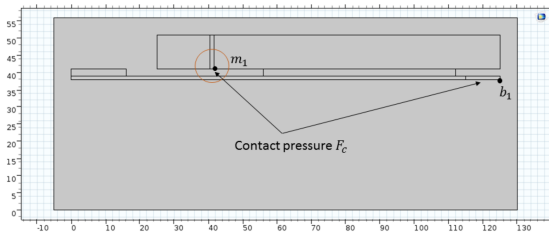


Fig. 5: Contact forces are imposed at some points of the head of the beam and of the mirror that can be in contact with the base and the stopper beam. The points  $b_1$  and  $m_1$  are used to plot displacement versus time in the following figures.

## 6. Homogenized model of the electrostatic equation in the MMA

The model derivation is based on the asymptotic method [4]. We start from the mathematical statement of the electrostatic equation in the MMA, we describe the assumptions regarding the geometry, the key operators for the asymptotic

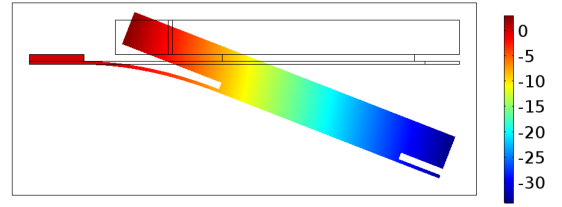


Fig. 6: Position of the mirror in its maximal displacement for a voltage exceeding the pull-in voltage.

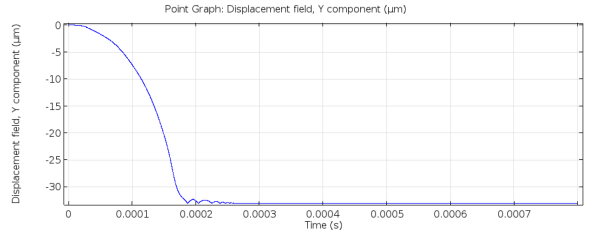


Fig. 7: Bounces of the mirror materialized by the trajectory of  $b_1$  in the case of a  $0.7\mu\text{m}$ -thick suspended beam.

model derivation, the asymptotic model itself, and its implementation in COMSOL Multi-physics.

### 6.1 Electrostatic equation

We consider a one-dimensional array of  $n$  cells with total length  $L$  as shown in Figure 9. Denoting by  $\ell$  the length of a cell, we express that the number of cells is large by considering that the length ratio  $\varepsilon = \ell/L$  is a small parameter. The asymptotic method yielding our model consists in establishing an approximation of the electrostatic equation in the sense of small values of  $\varepsilon$ . To underline the importance of this parameter in the problem, the fields and the domains are indexed by  $\varepsilon$ .

We assume that the array is subdivided into two parts where different voltages  $\pm V^{\varepsilon,1}$  and  $\pm V^{\varepsilon,2}$  are imposed, and we adopt the global notation  $\pm V^\varepsilon$  for the whole array. The governing equations of the electric potential  $\phi^\varepsilon$  in the vacuum domain is given as

$$-\operatorname{div}(\epsilon \nabla \phi^\varepsilon) = 0$$

in both subdomains with the imposed value  $\phi^\varepsilon = \pm V^\varepsilon$  on the mirrors and on the electrodes. Here  $\epsilon$  represents the electrical permittivity in vacuum. The external boundary condition on the other boundaries is the null-flux condition  $\nabla \phi^\varepsilon \cdot \mathbf{n}^\varepsilon = 0$  where  $\mathbf{n}^\varepsilon$  is the outward unit normal to the boundary. On the interface both the electrical potential and its normal flux are continuous.

### 6.2 Two-scale and zoom operators

To construct the model, we use the two-scale approximation technique presented in [4] which is generalized to account for boundary layer phenomena. We start by transforming the solution of the electrical potential  $\phi^\varepsilon$  defined on the physical domain into a function  $T\phi^\varepsilon$  defined on a two-scale domain  $\Omega^\sharp \times \Omega^1$ , see Figure 10, in which :  $\Omega^1$  is the microscopic cell deduced from any cell centered at the position  $x^\varepsilon$  by a translation by the vector  $-x^\varepsilon$  and a dilation by the factor  $1/\varepsilon$ , and  $\Omega^\sharp$  is the macroscopic domain that

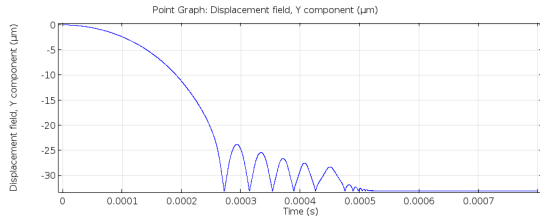


Fig. 8: Bounces of the mirror materialized by the trajectory of  $b_1$  in the case of a  $1\mu\text{m}$ -thick suspended beam.

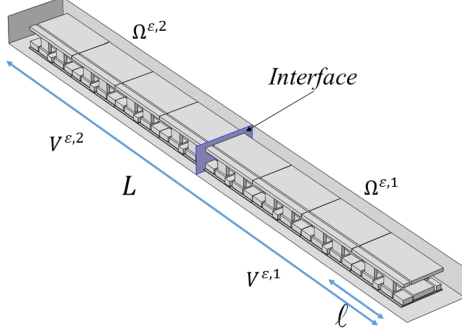


Fig. 9: Characteristics of the array regarding the asymptotic analysis: the ratio  $\ell/L$  of the cell length versus the array length and the voltage sources  $V^{\varepsilon,1}$  and  $V^{\varepsilon,2}$  in the two subdomains  $\Omega^{\varepsilon,1}$  and  $\Omega^{\varepsilon,2}$ .

is a segment, in the direction  $x_1$ , used for referencing the position of each cell of the array.

As will be seen in the following section, the approximation of  $T\phi^\varepsilon$  has a discontinuity at the interface between the two subdomains and does not satisfy the zero flux boundary conditions at the two ends of the array. For this purpose, correctors are introduced at the points presenting the approximation defects. Precisely, we use three operators  $T_b^{\text{int}}$  and  $T_b^\kappa$ , for  $\kappa \in \{0, L\}$ , of shift and zoom at the interface between the two subdomains and at both ends of the array. The shifts and zooms are chosen so that the transformations map any function defined on the nominal domain  $\Omega^\varepsilon$  into a function defined on the domains with first coordinate  $x_1^1 \in (-L^{\text{int}}/\varepsilon, (L - L^{\text{int}})/\varepsilon)$ ,  $[0, L^{\text{int}}/\varepsilon]$  and  $(-(L - L^{\text{int}})/\varepsilon, 0]$  respectively yielding  $x_1^1 \in (-\infty, +\infty)$ ,  $[0, +\infty)$  and  $(-\infty, 0]$  respectively when  $\varepsilon$  tends to zero.

### 6.3 The Homogenized model

Assuming that the two-scale transformations  $T\phi^\varepsilon \approx \phi^0$  and  $TV^\varepsilon \approx V^0$  when  $\varepsilon$  decreases, ie for a large number of cells, we can prove that  $\phi^0(x^\sharp, x^1)$  is solution of the fol-

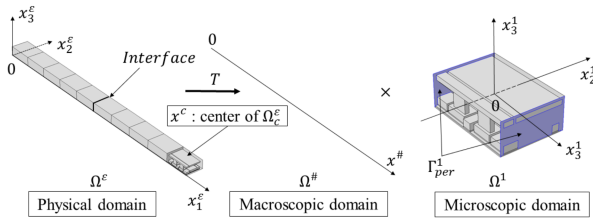


Fig. 10: Graphical view of the two-scale transform  $T$  mapping  $\Omega^\varepsilon$  into  $\Omega^\sharp \times \Omega^1$ .

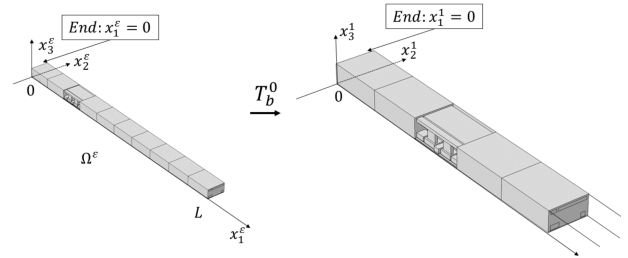


Fig. 11: Graphical view of the zoom operator  $T_b^1$  at the end  $x_1 = 0$ .

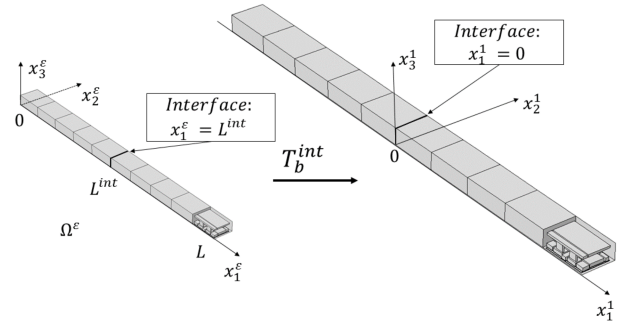


Fig. 12: Graphical view of the zoom operator  $T_b^{\text{int}}$  at the interface.

lowing equation posed in the microscopic domain for all  $x^\sharp \in \Omega^\sharp$ ,

$$-\operatorname{div}_{x^1} (\nabla_{x^1} \phi^0) = 0 \quad \text{in } \Omega^1, \quad (1)$$

with  $\phi^0 = \pm V^0$  on the mirrors and the electrodes,  $\phi^0$  and  $\nabla_{x^1} \phi^0$  satisfying periodic conditions in the lateral boundaries which normal vector is in the direction of the array and with zero flux condition on the other boundaries. The periodic boundary conditions are the origin of the approximation defects mentioned in the previous section. In order to construct the boundary layer corrections, we introduce the difference  $\phi_b^\varepsilon(x) = \phi^\varepsilon(x) - \phi^0(P^\sharp(x), (x - x^c)/\varepsilon)$  for each  $x$  belonging to the cell centered at  $x^c$  where  $P^\sharp$  is the projection operator from the domain  $\Omega^\varepsilon$  into  $\Omega^\sharp$ . This difference is zoomed at each point of approximation defect in order to determine the corrections by the asymptotic behaviors  $T_b^\kappa \phi_b^\varepsilon \approx \phi_b^\kappa$  and  $T_b^{\text{int}} \phi_b^\varepsilon \approx \phi_b^{\text{int}}$ , when  $\varepsilon$  decays, as well as the equations satisfied by limits  $\phi_b^\kappa$  and  $\phi_b^{\text{int}}$ ,

$$\begin{cases} -\operatorname{div}_{x^1} (\nabla_{x^1} \phi_b^{\text{int}}) = 0 \\ -\operatorname{div}_{x^1} (\nabla_{x^1} \phi_b^\kappa) = 0 \text{ for } \kappa = 0, L \end{cases} \quad (2)$$

in the three asymptotic regions as described in the previous section. In the three cases, the origin  $x_1^1 = 0$  corresponds to the location of the approximation defect. The boundary condition are that the jumps at the interface  $[\phi_b^{\text{int}} + \phi^0(L^{\text{int}}, x^1)]$  and  $[\partial_{x_1^1}(\phi_b^{\text{int}} + \phi^0(L^{\text{int}}, x^1))]$  are vanishing at  $x_1^1 = 0$ , as well as the normal flux  $\partial_{x_1^1}(\phi_b^0(x^1) + \phi^0(0, x^1))$  and  $\partial_{x_1^1}(\phi_b^L(x^1) + \phi^0(L, x^1))$  at the two ends of the array. Moreover, the three corrections  $(\phi_b^\kappa)_{\kappa=0,L}$  and  $\phi_b^{\text{int}}$  van-

ish on the mirrors and the electrodes, and satisfy zero flux boundary conditions on the other boundaries.

#### 6.4 Model implementation

In this subsection, the potentials  $\phi^0$ ,  $(\phi_b^\kappa)_{\kappa=0,L}$  and  $\phi_b^{int}$  are computed by solving the four equations (1) and (2). The main solution  $\phi^0$  is calculated on the microscopic domain  $\Omega^1$  for the two voltages  $V^0 = 20V$  and  $30V$ , see Figure 13 for a solution with  $V^0 = 20V$ . The computation of the boundary layer corrector  $\phi_b^\kappa$  is performed on domains starting from  $x_1^1 = 0$  and being two cell long only instead of infinite domains. It is possible to restrict simulation to one or two cells because the boundary layer correctors are exponentially vanishing and their value in the second cell is already negligible, see Figure 14. The same principle holds for the computation of the boundary layer corrector  $\phi_b^{int}$  at the interface which is computed on four cells, see Figure 15. The full solution is built by superimposing the periodic solution  $\phi^0$  and the three boundary layer correctors, see Figure 16.

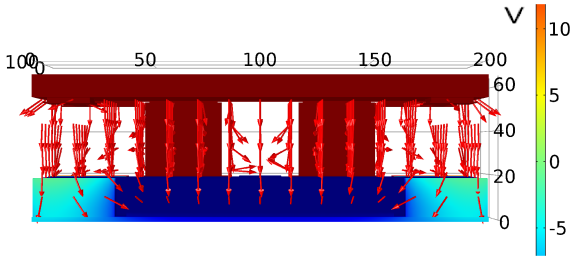


Fig. 13: Front view of a plot of  $\phi^0$  in the microscopic domain. The mirror and the pillars are in red while the bottom electrode is in blue. The imposed voltages are  $20V$  and  $-20V$ . The vector of electric field is materialized by red arrows. The electric field lines are vertical almost everywhere, with few tilted arrows visible on the edges; this means that the electric field is mainly localized in each cell, reducing to a very low value the crosstalk with neighboring cells.

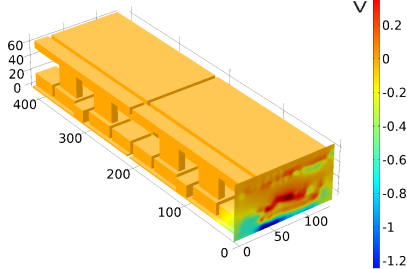


Fig. 14: One of the two boundary layer corrections  $\phi_b^0$  simulated in two cells at one end of the array.

**Conclusion** This paper presents advances in the modeling and simulation of the micro-mirror array MIRA. The principal contributions are, on the one hand, a model of the electrostatic field in one-dimensional arrays and on the other hand an analysis of the bounces of the mirror when a voltage exceeding the pull-in voltage is applied. We observe that the simulation time for a large array is related to the number of different voltages that are applied but not to its number of cells.

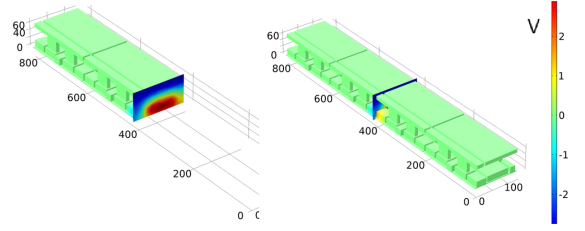


Fig. 15: Boundary layer correction  $\phi_b^{int}$  at the interface. It is computed in four cells centered to the interface.

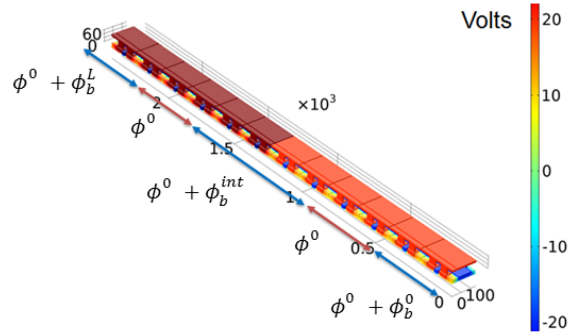


Fig. 16: Simulation result for a twelve-cell array. The imposed voltages are  $\pm 20V$  in the left part and  $\pm 30V$  in the right part. The figure shows the zones of superimposition of the solutions  $\phi^0$ ,  $\phi_b^\kappa$  and  $\phi_b^{int}$ .

## References

1. MD Canonica, F Zamkotsian, P Lanzoni, W Noell, and N De Rooij. The two-dimensional array of 2048 tilting micromirrors for astronomical spectroscopy. *Journal of Micromechanics and Microengineering*, 23(5):055009, 2013.
2. Michael David Canonica. *Large Micromirror Array Based on a Scalable Technology for Astronomical Instrumentation*. PhD thesis, ÉCOLE POLYTECHNIQUE FÉDÉRALE DE LAUSANNE, 2012.
3. Duy Duc Nguyen, Walid Belkhir, Nicolas Ratier, Bin Yang, Michel Lenczner, Frédéric Zamkotsian, and Horatiu Cirstea. A multi-scale model of a micro-mirror array and an automatic model derivation tool. In *Proceedings of the 16th Conference on EuroSimE IEEE Thermal, Mechanical and Multiphysics Simulation and Experiments in Micro/Nanoelectronics and Systems*, Budapest, Hungria, April, 2015.
4. M. Lenczner and R. C. Smith. A two-scale model for an array of AFM's cantilever in the static case. *Mathematical and Computer Modelling*, 46(5-6):776–805, 2007.
5. A El-Zafrany. Non-linear finite element analysis of solids and structures: Volume 2: Advanced topics. *Proceedings of the Institution of Mechanical Engineers*, 211(6):489, 1997.